Stability of particle propulsion by waveguide modes in the regimes where resonant states are formed

A. V. Maslov*
University of Nizhny Novgorod, Nizhny Novgorod, Russia
(Received 15 May 2015; published 10 September 2015)

Optical forces acting on dielectric particles inside waveguides are studied. The investigation is carried out within the framework of the two-dimensional model: a cylinder inside a parallel-plate waveguide with perfect metal walls. It is shown that although the appearance of resonant states can lead to a significant increase of backscattering and, therefore, the propelling force, the transverse force can either keep the particle in the location of the efficient propulsion or push it away. The propulsion and trapping regimes are related to the change of the resonant wavelength with particle location. Besides the geometrical and material parameters, the polarization of the incident mode is shown to significantly affect the particle dynamics. The relation of the resonant-state formation and Wood's anomalies in periodic gratings is also discussed.

DOI: 10.1103/PhysRevA.92.033814 PACS number(s): 42.50.Wk, 42.60.Da, 42.25.Fx, 41.20.Jb

I. INTRODUCTION

The incidence of an electromagnetic wave on a finite-size object leads to its scattering and the appearance of an electromagnetic force on the object. The correlation between the scattering and the force hints of the possibility of obtaining greater forces when the scattering possesses resonant features. The well-known examples of resonances include plasmon resonances in metallic particles, whispering gallery mode (WGM) resonances in large dielectric particles, and electric and magnetic resonances in high-permittivity particles.

Small dielectric particles with low or moderate values of the refractive index do not possess any pronounced intrinsic resonances. However, their manipulation by the electromagnetic field has many practical applications. For example, the real-life examples of small dielectric particles include blood cells or medical drags whose controlled transport and delivery are important for the biomedical industry. Although small particles do not have intrinsic resonances, they can form resonant states with the below-cutoff modes of metal waveguides and, therefore, their efficient manipulation can potentially be achieved.

The appearance of strong and narrow-band backscattering related to the formation of the resonant states allows one to design various microwave filters using dielectric inclusions inside hollow waveguides [1]. The resonant reflection in such systems should create resonant forces on the inclusions, by the nature of the momentum conservation. The appearance of resonant reflection from waveguide inhomogeneities, such as particles, is analogous to resonant reflection from periodic gratings (Wood's anomalies) where the resonant excitation of leaky modes takes place [2]. The surface modes supported by the periodic structure become leaking when the periodicity of the structure provides coupling between the surface modes and bulk waves. For large wavelengths, such coupling is absent and purely surface electromagnetic waves can exist. The guided-mode resonances offer opportunities to create mirrors and filters with resonant properties [3–5]. An increased absorption related to guided-mode resonances in an array of semiconductor nanowires can also be advantageous for photodetection [6]. The nanowires can potentially be replaced with semiconductor quantum wires that offer additional freedom in band-gap engineering but require taking into account anisotropy of their absorption [7]. The resonant scattering from periodic arrays in acoustics has also been studied [8] and is closely related to the presence of trapped modes formed by scatterers inside acoustical waveguides [9,10]. The design of offshore structures (for example, bridges or various platforms) consisting of finite periodic arrays of vertical columns should account for the possibility of resonant loads resulting from wave diffraction [11]. The resonant excitation of surface modes can also produce a strongly enhanced transmission through conducting screens with holes of various shapes [12].

The formation of a hybrid electromagnetic particle-waveguide state allows one to efficiently propel particles without intrinsic resonances, such as the WGM resonances used in Ref. [13]. The resonant force on a pointlike scatterer (cylinder) inside a parallel-plate waveguide (in two-dimensional geometry) for the transverse electric (TE) polarization was investigated in Ref. [14]. The trapping potential created by the lateral (transverse) force can keep the small particle at the maximum of the electric field of the TE_2 mode (off-center location) where the propelling force also peaks. The axial and lateral forces in the same geometry for high-index dielectric cylinders with small diameters were also investigated in Ref. [15]. The importance of accounting for the interaction with the walls and, therefore, the inadequacy of the gradient model for the lateral force based on the incident field only were also described [15]. Recently, the resonant propulsion of wavelength-size particles with rather small index contrast was demonstrated for the transverse magnetic (TM) polarization in the two-dimensional geometry and for the TE modes (with zero azimuthal number) in the three-dimensional geometry (spherical particles inside circular waveguide) [16]. The stability of propulsion inside a waveguide is especially interesting considering that a simple waveguide-resonator system with single resonance cannot possess stable optical equilibrium [17]. Strong transverse forces between nanorods in geometrically asymmetric silicon structures were also investigated recently [18].

From the experimental point of view, there has been significant interest in the manipulation of particles inside waveguiding structures. Reference [19] demonstrated laser guidance of solid particles and liquid droplets (diameters from 50 nm to 10 μm) inside a hollow-core (inner diameter from

*avmaslov@yandex.ru

10 to 50 μm) fiber capillary. The particles were confined by the radial intensity gradient force at the center. To overcome power losses in fiber capillaries, photonic crystal fibers (PCFs) were proposed and the guidance of 5 μm polystyrene spheres inside a 20 μm core of a PCF was demonstrated [20]. Forces created by the PCF modes (with core diameter 17 μm) were used to balance the fluidic counterflow acting on the particle (with diameters 1–3 μm) and control the particle movement by changing the optical power [21]. Laser propulsion of individual blood cells over distances of tens of centimeters inside liquid-filled PCF was also achieved [22]. Although there is clearly a significant experimental effort to manipulate the propulsion of particles in various confined geometries, there are no attempts so far to investigate the propulsion in the situation where resonant states are created.

This paper investigates the propulsion and trapping of particles that create the resonant states with the waveguide modes. The investigation is carried out using the two-dimensional model. The two-dimensional model is expected to give qualitatively similar results as the three-dimensional model, as demonstrated in Ref. [16], while being significantly easier to model numerically. The model includes both possible polarizations (TE and TM) and covers a large wavelength range, including the multimode regime. The investigation focuses on particles with rather small refractive index contrasts and sizes comparable to the operating wavelength. The boundary conditions at the particle surface related to the presence of the refractive index differ significantly from the Neumann boundary conditions used in acoustic scattering [8–11]. It is shown that although the creation of the resonant state leads to increased backscattering and the appearance of the resonant propelling force, the lateral force can either keep the particle stably in that transverse location or move it away with the simultaneous disappearance of the efficient propulsion. The resonant propelling forces are compared with that in free space. The regimes where the resonant propulsion can be stable and unstable are identified. It is also shown that the TE and TM polarizations of the incident mode give rise to different behaviors of the force peaks with change in particle location. The relation of the resonant-state formation and Wood's anomalies in periodic gratings is also discussed.

The paper is organized as follows. Section II introduces the physical model and the solution procedure. Section III discusses the results for the propulsion and trapping of the particles for various parameters. The relation of resonant propulsion and Wood's anomalies is discussed in Sec. IV. Section V gives the conclusion.

II. MODEL AND SOLUTION

The geometry of the two-dimensional problem is shown in Fig. 1(a). A waveguide mode is incident on the particle inside a parallel-plate waveguide and creates an optical force **F**. The parameters are the waveguide size L, the particle (cylinder) diameter D and its refractive index n_p, the location of the particle with respect to the center of the waveguide y_p, and the free-space wavelength $\lambda = 2\pi/k = 2\pi c/\omega$. Both polarizations are considered: TM (the magnetic field is along z) and TE (the electric field is along z). The fundamental TM_0 mode has no cutoff and has the largest momentum flow among all other modes at a fixed power and frequency.

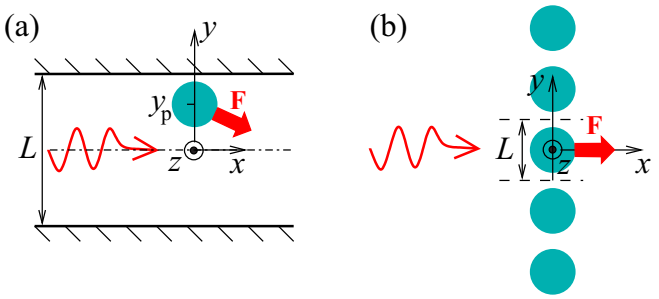

FIG. 1. (Color online) (a) Propulsion scheme: a waveguide mode is incident on a particle. (b) Periodic array of particles in which Wood's anomalies can be observed.

To find the force, we solve the scattering problem using the following analytical method. The polarization inside the particle is expanded into the cylindrical functions (which are the solution of the Helmholtz equation in uniform space) with unknown coefficients. The polarization current emits electromagnetic waves which are reflected by the boundaries at $y = \pm L/2$ and are incident back on the particle. The incident waves generate the total field inside the particle that corresponds to the assumed polarization. This gives a self-consistent condition for the coefficients in the polarization expansion. The linear system of equations for the coefficients is similar to that in Refs. [23,24]. After the coefficients are calculated, the components of the force can be found using formulas (11) and (12) from [24] that can be obtained either using the Lorentz formula or Maxwell tensor. The expansion coefficients allow one to find the amplitudes of the scattered guided waves. The scattering results were also verified using finite-difference time-domain (FDTD) simulations. The guided powers can alternatively be used to find the propelling (x component) of the force using the difference in the electromagnetic momentum flow of the incident and all scattered waves. The momentum flow M of a guided mode that has wave number h, frequency ω, and carries power P is given by

$$M = \frac{h}{\omega} P. \tag{1}$$

The transverse (y component) of force can be calculated by using the approach described in Ref. [15],

$$F_y = \frac{\omega}{c} \sum_n P_n \frac{\partial \varphi_n}{\partial y_p}, \tag{2}$$

where φ_n is the phase and P_n is the power of the nth scattered guided mode. The sum in (2) is performed over all excited modes. The calculation of each force component using the two methods was implemented numerically and the results matched for all of the cases studied in the present paper. To describe particle trapping, it is also convenient to introduce the trapping potential U using

$$F_y = -\frac{\partial U}{\partial y_p}. \tag{3}$$

In the calculations, the constant level in the trapping potential U is chosen such that $U = 0$ at $y_p = 0$. The minima of the trapping potential define the particle positions y_p where propulsion is stable. In practice, it is convenient to plot the

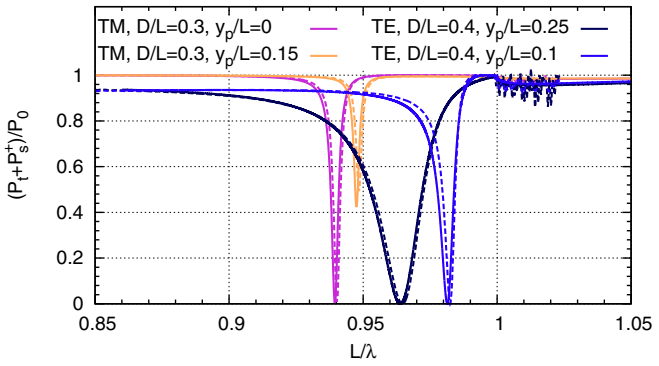

FIG. 2. (Color online) Comparison of the transmitted power calculated using the analytical approach (solid lines) and FDTD approach (dashed lines) for both polarizations (TE and TM), several values of the particle size (D/L), and displacement (y_p/L), as indicated in the figure.

normalized force $cF_{x,y}/P_0$ and the potential $cU/(LP_0)$, where P_0 is the power of the incident guided mode.

III. PROPULSION AND TRAPPING INSIDE WAVEGUIDES

The analysis includes both possible polarizations, TE and TM. The lowest modes, TE_1 and TM_0, are used as the incident modes. The refractive index for the particle is set to $n_p = 1.3$, but the size D and location y_p change.

The correctness of the numerical implementation of the analytical solution is initially verified by comparison of its results with that of an in-house developed FDTD code. Figure 2 shows the total transmitted power, which consists of the power in the same transmitted mode (P_t) and in the higher-order modes (for $L/\lambda > 1$) propagating in the $+x$ direction (P_s^+), calculated by the two methods. Both polarizations and several values of D/L and y_p/L are used. The results agree well in all cases. The small difference in the positions of the transmission dips can be attributed to a discretization error for the refractive-index distribution related to a finite size of the FDTD cell ($\Delta x = L/40$). The fast oscillations just above $L/\lambda = 1$ observed in the FDTD results are most likely related to the very slow group velocity of the excited mode just above its cutoff and perhaps its rather weak absorption by the absorbing layers at the ends of the simulation domain. The simulations using the analytical method are significantly faster than using the FDTD method and do not produce numerical artifacts. Since the calculation of force using the Lorentz formula or Maxwell tensor requires the knowledge of the field in the frequency domain or complex transmission coefficients, the FDTD implementation becomes somewhat less attractive. Certainly, the use of the analytical method is limited to simple geometries, such as shown in Fig. 1, but this is sufficient to study the basic features of the particle propulsion.

The propelling force in the spectral range $0.5 < L/\lambda < 2$ is shown in Fig. 3. For the TE polarization and $D/\lambda = 0.25$, one can see the peaks of the propelling force that correspond to the formation of resonant states just below the cutoffs $L/\lambda = 1,\ 1.5,\ 2$. The resonant state near $L/\lambda = 1$ corresponds to the excitation of the TE_2 mode. Since it has a node of the electric field in the center of the waveguide, the excitation of the

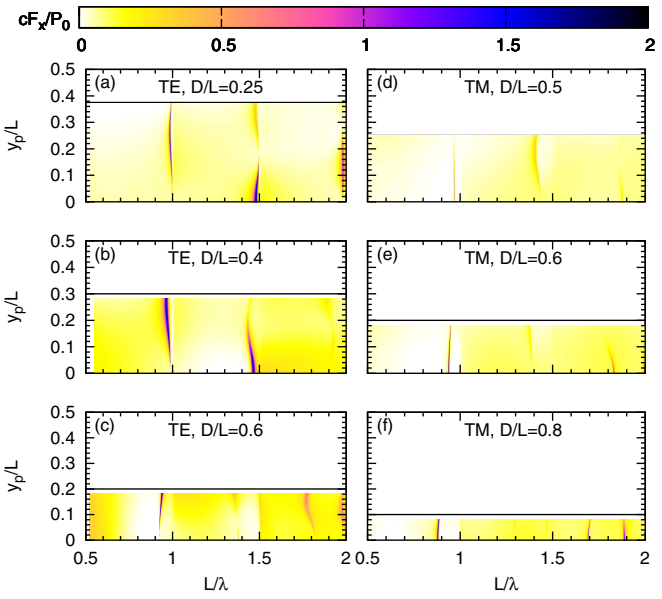

FIG. 3. (Color online) Color map of the propelling force cF_x/P_0 on the particle as a function of y_p/L and L/λ for (a)–(c) TE and (d)–(f) TM polarizations and several sizes, D/L. The horizontal solid lines denote the largest y_p/L the particle can reach due to its finite size.

resonant state vanishes at $y_p = 0$. In contrast, the excitation of the resonant state near $L/\lambda = 1.5$ (cutoff for TE_3) has a maximum near $y_p = 0$. As the particle size increases to $D/L = 0.4$, the peaks become wider and their shifts with the particle position y_p become more noticeable. At even larger size, $D/L = 0.6$, the peaks, however, become less pronounced.

For the TM polarization, the resonant peaks of the propelling force become noticeable only for larger sizes as compared to the TE case. The peaks reach the maximum values allowed by the momentum conservation but remain rather narrow. The peak just below $L/\lambda = 1$ exists even when the diameter of the particle reaches the width of the waveguide.

The smaller width of the peaks in the TM case as compared to the TE case can be attributed to smaller values of the induced polarization (and, thus, less pronounced scattering) for the particles of the same sizes and refractive indices. Figure 4 compares the cross sections for radiation pressure and scattering as functions of D/λ for $n_p = 1.3$ when the plane waves of TE or TM polarization are incident on the cylinder in free space. For example, at $D/\lambda = 0.6$, one has $\sigma_{sc}^{TM}/\sigma_{sc}^{TE} \approx 0.66$ and $\sigma_{rp}^{TM}/\sigma_{rp}^{TE} \approx 0.48$. In particular, for small sizes $D \ll \lambda$, one can derive asymptotic formulas

$$\frac{\sigma_{sc}^{TE}}{D} \approx \frac{\pi^2}{4}\frac{(\varepsilon-1)^2}{2}(kR)^3, \tag{4a}$$

$$\frac{\sigma_{sc}^{TM}}{D} \approx \frac{\pi^2}{4}\frac{(\varepsilon-1)^2}{(\varepsilon+1)^2}(kR)^3, \tag{4b}$$

where $\varepsilon = n_p^2$ is the permittivity, $R = D/2$ is the radius, and $k = \omega/c$ is the wave number. The asymptotic formulas show explicitly that $\sigma_{sc}^{TE} > \sigma_{sc}^{TM}$. The radiation pressure cross section in Fig. 4 remains smaller than D: $\sigma_{rp}^{TE,TM}/D < 1$. On the other hand, the force on the particle inside the waveguide can reach $cF_x/P_0 = 2$ for the TM polarization (see Fig. 3),

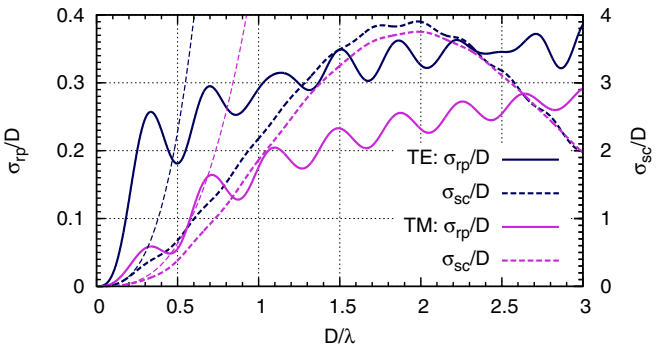

FIG. 4. (Color online) Radiation pressure (solid lines, left axis) and scattering (dashed lines, right axis) cross sections for a cylinder with $n_p = 1.3$ in free space as functions of the size parameter D/λ for plane waves with TE and TM polarizations. The thin dashed lines show the asymptotic behavior for the scattering cross sections in the limit $D/\lambda \ll 1$ given by Eq. (4).

which corresponds to the radiation pressure cross section $2L$ that is significantly larger than the particle size D.

Let us now investigate more closely the properties of the resonant states for various parameters and polarizations. Figure 5 summarizes the properties of the resonant peak just below $L/\lambda = 1$ for $D/L = 0.4$ and the TE polarization. The resonant state is rather broad when the particle is around $y_p/L = 0.25$ and decreases if the particle moves to the center $y_p/L = 0$; see Figs. 5(a) and 5(b). However, the peak height remains essentially the same and reaches $cF_x/P_0 \approx 1.7$. This value is consistent with the total reflection of the incident mode that has wave number $h = (\omega/c)\sqrt{3}/2$ at $L/\lambda = 1$; see also Eq. (1). Figure 5(c) simultaneously shows the trapping potential and the propelling force at several values of the frequency parameter L/λ. As one starts at the large wavelength side, $L/\lambda = 0.96$, the particle is trapped near $y_p/L \approx 0.27$ where the force also has a maximum, $cF_x/P_0 \approx 1.5$. Then, at $L/\lambda = 0.9635$, the trapping potential becomes slightly deeper and the propelling force forms a plateau of height $cF_x/P_0 \approx 1.7$ in the area that corresponds to the minimum of U. Thus, one can expect that the particle can be trapped efficiently and propelled at the same time. Further increase of L/λ leads to further deepening of the trapping potential U. However, now U becomes very flat near its minimum and, therefore, the particle can move rather freely in the transverse direction. Moreover, the maximum of propulsion moves away from the minimum of U to the region of smaller y_p/L. This means that the propulsion of the particle takes place at the location from which the particle will move away due to the transverse force. Due to the weakness of the trapping potential the particle can, however, reach the locations where the propulsion is large, but then will move back to the regions where the propulsion is very weak.

Figure 6 summarizes the resonant propulsion for larger particles, $D/L = 0.6$, for the TE polarization. The maximum of the propelling force reaches practically the same value as for $D/L = 0.4$. However, the behavior of the particle changes drastically; see Fig. 6(c). For all values of L/λ, the trapping potential has its minimum near $y_p = 0$ where there is no propulsion. Strong propulsion is only possible at the locations

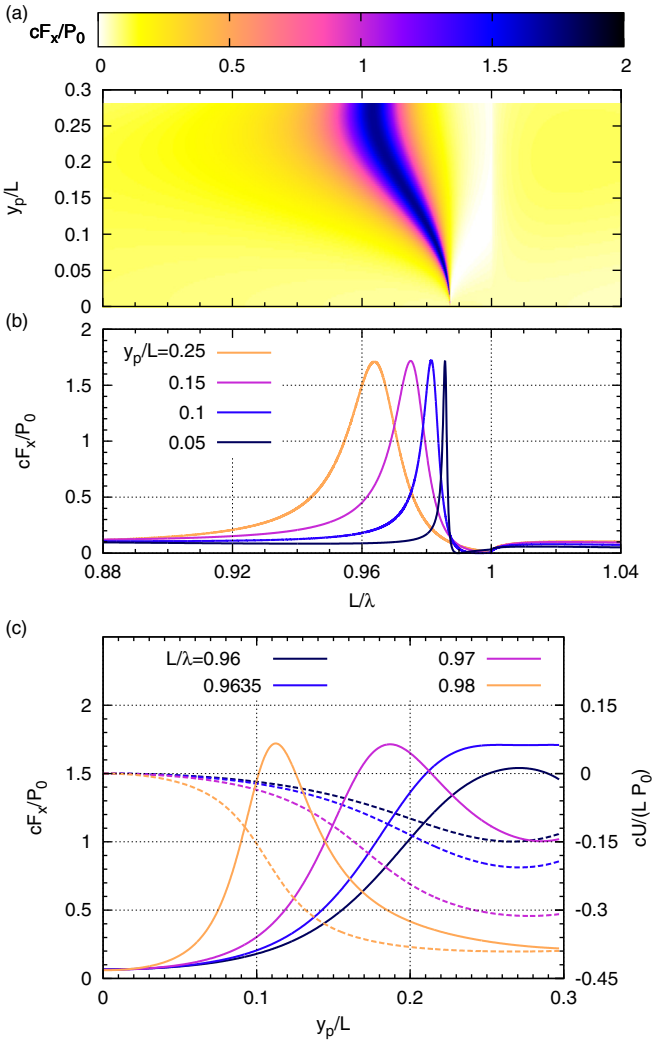

FIG. 5. (Color online) Properties of the resonant state for the TE polarization, $D/L = 0.4$, $n_p = 1.3$. (a) Color map of the propelling force cF_x/P_0 as a function of the frequency parameter L/λ and particle position y_p/L. (b) cF_x/P_0 as a function of L/λ for several values of y_p/L. (c) cF_x/P_0 (solid lines, left y axis) and corresponding transverse potential $cU/(LP_0)$ (dashed lines, right y axis) as functions of y_p/L for several values of L/λ.

that also have large transverse forces (gradient of U) which push the particle to the center, $y_p = 0$. The absence of trapping can perhaps be attributed to the large size of the particle that cannot move to the region $y_p/L > 0.2$, where the stable propulsion can be achieved as in Fig. 5. Therefore, the particle cannot be trapped and propelled simultaneously.

Figure 7 summarizes the resonant propulsion for particles with $D/L = 0.6$ and for the TM polarization. The peak of the force reaches $cF_x/P_0 = 2$ when the particle is at the center of the waveguide, $y_p = 0$. However, when $y_p/L \neq 0$, the peak becomes smaller. The propulsion of the particle can be stable. Indeed, the minima of the trapping potential for $L/\lambda = 0.938$, 0.9395 correspond to the maxima of cF_x/P_0. With a further increase of L/λ, however, the maximum of the trapping potential remains at $y_p = 0$ but the peak of the propelling force moves to larger y_p. The values $L/\lambda = 0.941$, 0.945

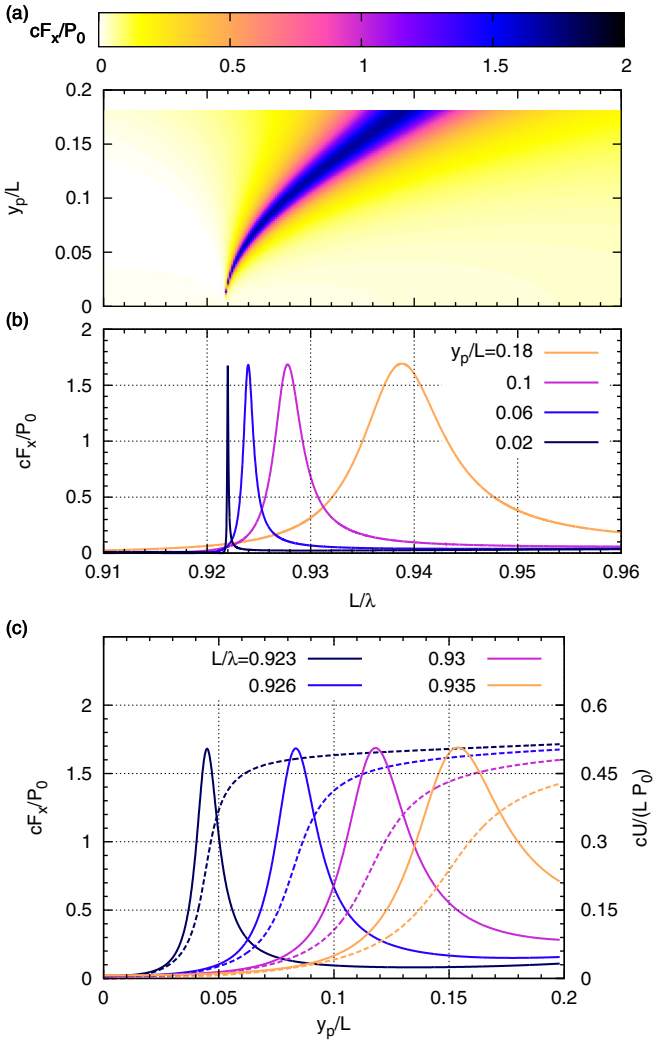

FIG. 6. (Color online) Same as Fig. 5, but for larger particle $D/L = 0.6$.

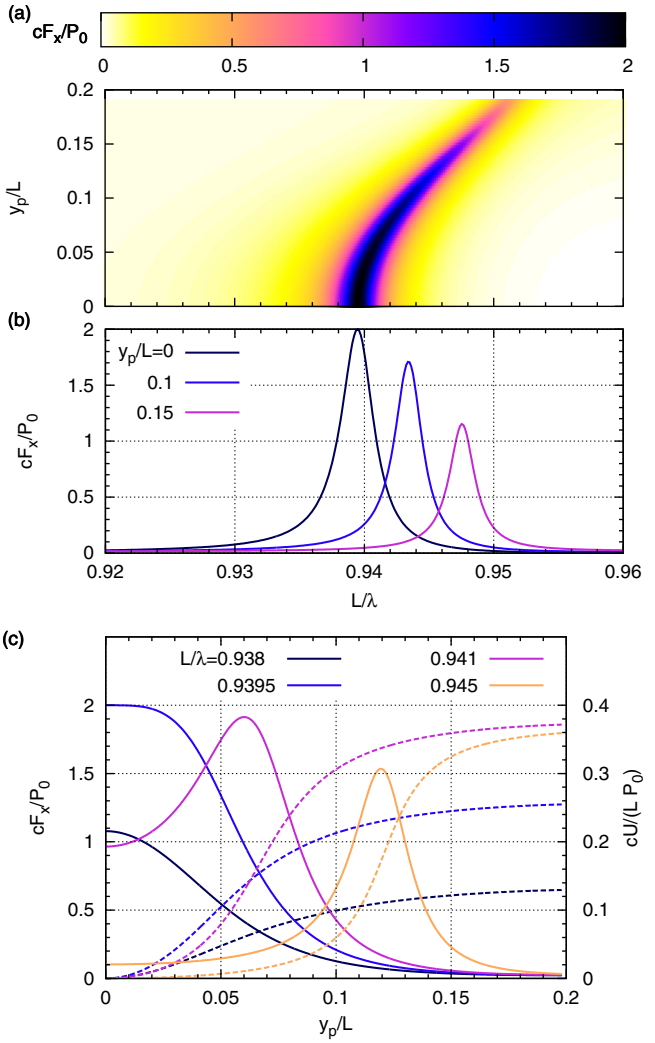

FIG. 7. (Color online) Same as Fig. 5, but for $D/L = 0.6$ and the TM polarization.

correspond to the existence of unstable propulsion, similar to the case shown in Fig. 5.

Thus, depending on the parameters (such as n_p, D, L, λ), the propulsion of the particle can be stable or unstable. In the stable regime, the maximum of the propelling force coincides with the minimum of the trapping potential. Thus, any deviation from that position will bring the particle back. In the unstable regime, the maximum of the propelling force corresponds to the presence of a transverse force that pushes the particle away to the locations where the propulsion is weaker or even is practically absent. For the TE polarization, the width of the resonant peak of cF_x/P_0 as a function of L/λ depends strongly on the location of the particle y_p/L, while its maximum remains practically unchanged; see Figs. 5(b) and 6(b). In contrast, for the TM polarization, the maximum of cF_x/P_0 changes with the particle location y_p/L, but the width of the peak does not change significantly; see Fig. 7(b).

IV. RESONANT FORCES AND WOOD'S ANOMALIES

There is a close relation between the existence of resonant states formed by particles inside waveguides and peculiar properties of wave scattering by periodic structures. Let us take, for example, an array with period L of cylinders with dielectric constant n_p and diameter D; see Fig. 1(b). The scattering by the array can be calculated using the same approach as for particles inside a waveguide. The only change is that the multiple reflections from the walls are replaced by the waves coming from various particles in the array. The guided modes in the case of a waveguide become various scattering orders in the case of an array. The normal incidence of the TM wave, which has its magnetic field along z, on an array is equivalent to the incidence of the TM_0 mode on a particle in the center of the parallel-plate waveguide with perfect metal walls, as in Sec. III. Indeed, the conditions that $H_z(y)$ must be periodic along y and symmetric, $H_z(-y) = H_z(y)$, give the requirement of the vanishing normal derivative of H_z at $y = \pm L/2$ that leads to vanishing E_x. The normal incidence of the TE wave, which has its electric field along z, on an array is equivalent to the incidence of the lowest mode of the waveguide with walls made of a perfect magnetic conductor, rather than a perfect electric conductor. The scattering of the normally incident TE wave on an array, therefore, differs from

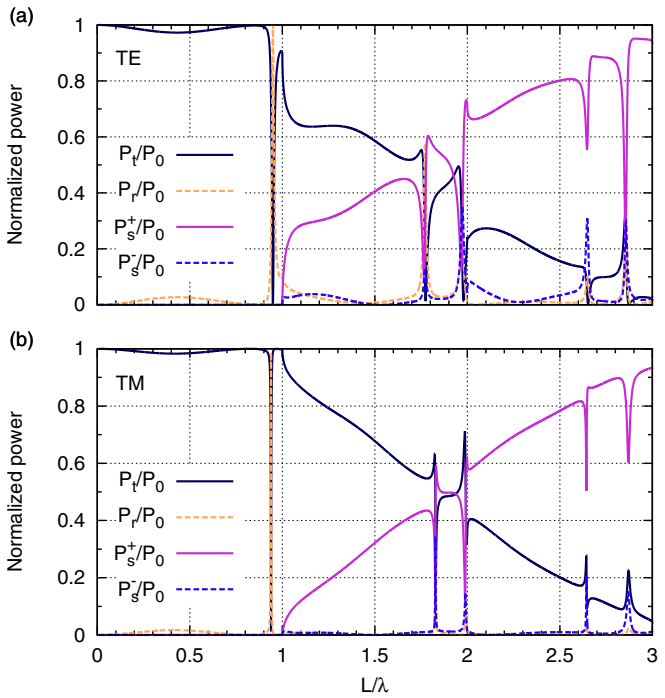

FIG. 8. (Color online) Scattering of a normally incident plane wave by an array of cylinders for two polarizations: (a) TE and (b) TM. The powers are normalized to the incident power P_0. The parameters are $D/L = 0.6$, $n_p = 1.3$.

the case of the waveguide with perfect metal walls that was investigated in Sec. III. The incidence of the TE_1 mode for a particle in the center of the waveguide with perfect metal walls is equivalent to the incidence of two oblique plane waves on an array.

Here we study and compare the scattering of normally incident TE and TM waves by the periodic array of circular scatterers. The case of scatterers with rectangular cross section was considered in Ref. [25] using perturbative and purely numerical approaches. The incident wave produces transmitted and reflected waves (zero-order scattering) as well as waves that are scattered under some angles with respect to the incidence direction. The number of the scattered waves depends on the parameter L/λ. Figure 8 shows the transmitted (P_t), reflected (P_r), and scattered ($P_s^{\pm}$) powers propagating in the $\pm x$ directions. For $L/\lambda < 1$, only the transmitted and reflected waves exist. New scattered beams appear when L/λ exceeds an integer. There is a clear resonance just below the appearance of the first scattering order. The width of the resonance is smaller in the TM case, but the resonances are still clearly present, unlike in the weakly scattering regime [25]. In addition, there are similar resonances at large values of L/λ.

The resonant peaks are related to the forced excitation of leaky waves supported by the periodic array and correspond to one type of Wood's anomalies [2]. The resonance effects may take place near the Raleigh wavelength or rather away from it. Besides the resonance anomaly, Fig. 8 also demonstrates the other type of Wood's anomaly—a rapid variation of the powers corresponding to the onset of new spectral orders. We can therefore conclude that the resonant scattering for particles in waveguides is analogous to the resonant Wood's anomalies. However, the exact position of the resonance for particles inside waveguides depends strongly on the boundary conditions as well as on the transverse position of the particle. Moreover, the displacement of the particle from the waveguide center breaks the symmetry of the problem—a situation that cannot be directly modeled using a periodic array.

V. CONCLUSION

To conclude, the force on a particle inside a waveguide was investigated in the regimes where the particle forms resonant states with the below-cutoff modes. The investigation was carried out within the framework of the two-dimensional model: a cylinder inside a parallel-plate waveguide with perfect metal walls. The presence of a resonant state can give rise to a total reflection of the incident mode. The propelling force, therefore, becomes much larger than for the same particle in free space. However, the particle motion under the large propelling force is also affected significantly by the transverse force. Two regimes were identified. In the first regime, the stable transverse trapping also corresponds to the efficient propulsion. Any random deviation from the stable location leads to the reduction of the propelling force. In the second regime, the stable transverse location corresponds to a rather weak propelling force. A deviation from it can temporarily increase the propelling force, but the created transverse force will cause the particle to return to its stable transverse location. Sudden jumps in the propulsion dynamics have been observed experimentally in somewhat different geometry: when a WGM is excited in the particle located near a fiber taper [26,27]. The polarization of the incident mode (TE or TM) was also shown to have a significant effect on the dependence of the propelling force on the parameter L/λ. For the TE polarization, the peaks of the propelling force change their width with the particle location but not their height. For the TM polarization, the peaks change their height with the particle location but not their width. The resonant scattering of the guided modes on particles in the center of the waveguide also has a direct analogy to Wood's anomalies in periodic gratings.

ACKNOWLEDGMENTS

The author is grateful to V. N. Astratov and M. I. Bakunov for discussions. This work was supported by the Ministry of Education and Science of the Russian Federation through Agreement No. 14.578.21.0041 (RFMEFI57814X0041).

[1] J. N. Sahalos and W. Vafiadis, IEEE Trans. Microwave Theory Tech. **33**, 1165 (1985).
[2] A. Hessel and A. A. Oliner, Appl. Opt. **4**, 1275 (1965).
[3] L. Mashev and E. Popov, Opt. Commun. **55**, 377 (1985).

[4] R. Magnusson and S. S. Wang, Appl. Phys. Lett. **61**, 1022 (1992).
[5] A. D. Bristow, V. N. Astratov, R. Shimada, I. S. Culshaw, M. S. Skolnick, D. M. Whittaker, A. Tahraoui, and T. F. Krauss, IEEE J. Quantum Electron. **38**, 880 (2002).
[6] A. Hosseinnia and N. Anttu, Photon. Res. **3**, 125 (2015).
[7] A. V. Maslov and C. Z. Ning, Phys. Rev. B **72**, 161310 (2005).
[8] C. M. Linton and I. Thompson, Wave Motion **44**, 165 (2007).
[9] M. Callan, C. M. Linton, and D. V. Evans, J. Fluid Mech. **229**, 51 (1991).
[10] R. Porter and D. V. Evans, J. Fluid Mech. **386**, 233 (1999).
[11] H. D. Maniar and J. N. Newman, J. Fluid Mech. **339**, 309 (1997).
[12] B. A. Munk, *Metamaterials: Critique and Alternatives* (Wiley, New York, 2009), Sec. 1.12.6.
[13] A. V. Maslov and M. I. Bakunov, Opt. Lett. **39**, 2823 (2014).
[14] R. Gómez-Medina, P. San José, A. García-Martín, M. Lester, M. Nieto-Vesperinas, and J. J. Sáenz, Phys. Rev. Lett. **86**, 4275 (2001).
[15] Z. Wang and P. T. Rakich, Opt. Express **19**, 22322 (2011).
[16] A. V. Maslov and M. I. Bakunov, Opt. Lett. **40**, 1806 (2015).
[17] V. Intaraprasonk and S. Fan, Opt. Express **21**, 25257 (2013).
[18] J. Zhang, K. F. MacDonald, and N. I. Zheludev, Opt. Lett. **39**, 4883 (2014).
[19] M. J. Renn, R. Pastel, and H. J. Lewandowski, Phys. Rev. Lett. **82**, 1574 (1999).
[20] F. Benabid, J. C. Knight, and P. St. J. Russell, Opt. Express **10**, 1195 (2002).
[21] T. G. Euser, M. K. Garbos, J. S. Y. Chen, and P. St. J. Russell, Opt. Lett. **34**, 3674 (2009); **35**, 2142 (2010).
[22] S. Unterkofler, M. K. Garbos, T. G. Euser, and P. St. J. Russell, J. Biophoton. **6**, 743 (2013).
[23] A. V. Maslov, V. N. Astratov, and M. I. Bakunov, Phys. Rev. A **87**, 053848 (2013).
[24] A. V. Maslov, Phys. Rev. A **90**, 033825 (2014).
[25] A. Maurel, S. Félix, J.-F. Mercier, A. Ourir, and Z. E. Djeffal, J. Euro. Opt. Soc. Rap. Public. **9**, 14001 (2014).
[26] Y. Li, O. V. Svitelskiy, A. V. Maslov, D. Carnegie, E. Rafailov, and V. N. Astratov, Light Sci. Appl. **2**, e64 (2013).
[27] Y. Li, A. V. Maslov, N. I. Limberopoulos, A. M. Urbas, and V. N. Astratov, Laser Photon. Rev. **9**, 263 (2015).